IEEE Access
Multidisciplinary | Rapid Review | Open Access Journal

Received 30 May 2024, accepted 20 July 2024, date of publication 29 July 2024, date of current version 6 August 2024.

Digital Object Identifier 10.1109/ACCESS.2024.3434635

RESEARCH ARTICLE

Fault Monitoring and Diagnosis of Motor Operation Status Based on LBP-SVM

WENCHANG WU
Department of Automotive and Electromechanical Engineering, Xinyang Vocational and Technical College, Xinyang 464000, China
e-mail: wenchang505@163.com

ABSTRACT As an important power device in modern industry, electric motor plays a vital role in the production process. In the face of the expanding scale of the motor system and the increasing complexity of the working environment, the study proposes a new model for motor fault diagnosis based on local binary patterns and support vector machines. By analyzing the motor operation data, while extracting texture features using local binary patterns, and accurately classifying and diagnosing by support vector machines, the study aims to improve the accuracy and real-time performance of fault detection. Experimental results show that the diagnostic model is able to complete the feature classification in as little as 200 seconds, and the fault classification accuracy can reach up to 97%. The model's fault prediction has the smallest mean square error of 0.017, the smallest root mean square error of 0.214, and the smallest mean absolute error of 0.011. From the above data, it can be seen that the proposed method of the study can significantly improve the efficiency and accuracy of fault detection. The contribution of the study is to propose an effective method for motor fault monitoring and diagnosis, which provides important support for motor fault prevention and maintenance, and also lays a new theoretical foundation for the development of motor fault diagnosis technology.

INDEX TERMS Fault diagnosis, Gaussian kernel function, local binary mode, motor system, support vector machine.

I. INTRODUCTION

In modern industry, the reliability and efficiency of motors are crucial, and fault diagnosis has become a key technology to ensure the normal operation of motors [1]. For this field, researchers at home and abroad have successively proposed many solutions. For example, the combination of the latest advances in the Internet of Things and big data technology makes motor fault detection realize real-time monitoring and remote diagnosis [2]. The real-time collection of motor operation data through IoT technology and the use of big data analysis technology for data mining and pattern recognition can realize timely warning and diagnosis of motor failure. However, the large amount of data generated by motors in the field environment poses challenges to data transmission, storage and processing, especially in scenarios with high real-time requirements, and the performance and stability of edge computing still need to be further improved. In recent years, significant achievements have been made in the field of motor condition monitoring and fault diagnosis using image processing techniques and machine learning. In particular, Local Binary Pattern (LBP) and Support Vector Machine (SVM) have gained widespread attention for their powerful feature extraction and classification capabilities [3]. Although AI classifiers utilizing deep learning have demonstrated excellent performance in several fields, deep learning methods require a large amount of labeled data and computational resources when dealing with motor fault diagnosis, which is often a major limitation in practical applications [4]. In contrast, LBP, as an effective texture analysis method, can extract key features from motor operation data, while SVM, with its superior classification performance and low computational complexity, performs better in small-sample learning scenarios. In addition, although Local Ternary Pattern (LTP) provides richer information for the extension of LBP, LBP still has its unique advantages in simplifying computation

The associate editor coordinating the review of this manuscript and approving it for publication was Xueguang Zhang.

and reducing model complexity. The study focuses on several common failure modes in motor operation, including bearing damage, rotor unbalance and stator winding failure. Vibration signals, temperature variations and current anomalies during motor operation are collected and analyzed. By combining LBP and SVM, a novel motor fault monitoring and diagnosis model is proposed, aiming to improve the diagnostic accuracy and efficiency, while reducing the dependence on large-scale training data and providing more effective technical support for motor fault prevention and maintenance. Through experimental validation, the extraction time of the proposed model under the study can be as short as 200 seconds, and the prediction accuracy is close to 97%, which not only outperforms the existing methods in terms of feature extraction speed and diagnosis accuracy, but also demonstrates the robustness under different working conditions, which is of great significance in promoting the development of motor fault diagnosis technology.

II. RELATED WORKS

The widespread use of electric motors in industry makes motor operation fault monitoring and diagnosis crucial. Motor failures not only lead to equipment downtime and production disruption, but also may cause greater accidents and losses. Therefore, timely detection and resolution of motor faults are crucial to ensure production continuity and equipment reliability. Jiang et al. proposed a strong robust diagnostic strategy based on d-q axis current signals in order to diagnose open-circuit faults in a novel fault-tolerant drive motor system. The strategy can perform fault diagnosis work properly in an environment with very few independent power supplies and converters. Simulation experimental results show that the strategy can overcome the early warning problem of motor fault diagnosis under sudden load changes or light load conditions [5]. Afrasiabi et al. found that existing convolutional neural networks still have some deficiencies in diagnosing motor faults, in view of which the research team proposes a single-module convolutional neural network incorporating a Gabor filter. Experimental results show that this novel network has more excellent performance than feedforward neural networks and general neural networks [6]. Fu et al. proposed a multi-modal neural network algorithm incorporating dynamic routing in order to improve the efficiency of existing methods for fault diagnosis of induction motors. The method introduces a dynamic routing algorithm at the decision layer to assign appropriate weights to different modes in an adaptive manner. The experimental results show that the novel diagnostic method is effective and robust compared to the same type of methods [7]. In order to reduce the cost of motor operation faults, Behloul et al. proposed a novel motor defect detection technique after combining local ternary mode and gray level co-occurrence matrix. Experimental results show that this technique has more obvious detection efficiency and lower cost compared to other more popular multiclassification fault detection techniques [8]. In order to further explore the value of combining LBP and SVM in the field of electric motor faults, Hernandez-Ramirez et al. constructed a machine-learning fault detection method by utilizing difference histograms and SVM. The experimental results showed that the detection accuracy of the method was up to 98.16% [9].

With the development of digital image processing and feature classification techniques, local binary patterns and support vector machines have gradually come into the public's view and have achieved certain results in many application areas respectively. Basaran and Fidan found that variations in vibration characteristics provide indicators about the type of failure and can be used for click fault detection. Therefore, the research team proposed a novel detection model combining LBP and SVM. Experimental results showed that the model was found to be more successful in classifying motor faults with an accuracy of 96.7 when compared with other popular machine learning algorithms [10]. Saidi et al. found that existing LBPs consume a large amount of time and training data during texture analysis, so the research team proposed a new method that incorporates circular partial local binary patterns. The experimental results show that the accuracy test result of this method in Outex 10 dataset reaches 98.7% [11]. Zhu et al. In order to improve the accuracy of earthquake magnitude estimation, a new magnitude estimation model is proposed after combining migration learning and SVM. Simulation experiments show that the estimation errors of event magnitude by the proposed model are within plus or minus 0.3 magnitude units in five tests of seismic events [12]. Qin et al. In order to more accurately measure the water holding capacity of in situ loess soil samples with different soil textures, a prediction model for water retention parameters in the low-water-table range is proposed by combining the Particle Swarm Algorithm and SVM. The experimental results showed that the absolute, relative and root mean square errors between the predicted and tested values of the model were less than 0.0153, 0.1071 and 0.0633, respectively. Indicating that the overall performance of the model was effective and stable, and the prediction was better [13].

In summary, the state-of-the-art technologies cover a wide range of fields, and some of the prominent results include the application of deep learning methods, the combination of IoT and big data technologies, and the development of digital image processing and feature classification techniques. These techniques have brought innovations and advances in the field of motor fault detection, where motor fault detection methods combining LBP and SVM have made significant contributions in improving detection efficiency and accuracy. In view of this, the study continues to optimize the feature extraction of LBP and combines SVM to provide more effective theoretical support for the technological development in this field.

III. CONSTRUCTION OF MOTOR OPERATION FAULT MONITORING AND DIAGNOSIS MODEL BASED ON LBP-SVM

In order to build a more effective and stable motor fault diagnosis model, the first section of the study firstly analyses

the motor fault signals and their features, and provides a basis for the subsequent model construction by means of enhancing the signal features. The second section of the study then combines LBP and SVM to propose a novel motor fault diagnosis model.

A. MOTOR OPERATION FAULT FEATURE EXTRACTION AND SIGNAL ENHANCEMENT

Electric motors are widely used equipment in industrial production, and their failure may lead to serious consequences such as production interruptions, losses and safety accidents. Therefore, accurate motor fault diagnosis is of great significance to ensure the safety and stability of production. Traditional motor fault diagnosis methods are mainly based on expert experience and monitoring of sensor data, but there are problems such as long diagnosis time, low accuracy and high cost [14]. The general motor fault diagnosis system is shown in Figure 1.

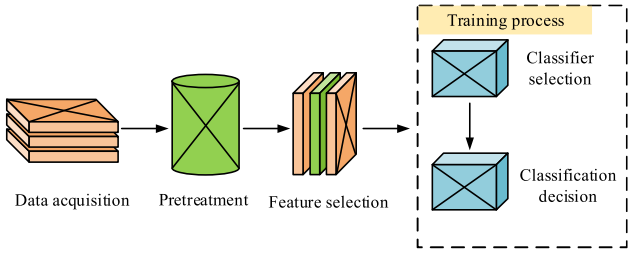

FIGURE 1. Motor fault diagnosis system.

As can be seen from Figure 1, the method is mainly divided into four parts: data acquisition, pre-processing, feature extraction and diagnostic analysis. Motor operating data is first collected, then preprocessed to ensure accuracy, followed by extraction of features to describe the motor state, and finally diagnostic analysis to determine the presence of faults. And the current method is mainly combined with neural algorithms for diagnosis, although the diagnosis speed is fast and the accuracy rate is high, but there is the problem of high cost of neural network training and complex training. Combined with the fact that the object of this research is the electric motor, it is generally difficult to obtain a large amount of fault data to train the model under normal conditions, and the use of time-frequency heat maps of signals for fault warning and diagnosis is more intuitive, computationally efficient, and better fitted to a specific problem compared to neural algorithms. So the research tries to use the time-frequency heat map of the signal to carry out fault warning and diagnosis [15]. The time-frequency thermogram of the signal must firstly be plotted by analysing the spectrum of the acquired data signal in order to preferentially obtain certain dynamic features that are representative in the time domain. The general time-frequency feature visualization method is the wavelet transform, which is better compared to the quadratic distribution because the wavelet transform has better time-frequency resolution and better adaptability to non-smooth signals, and can capture the time-frequency features of the signal more accurately. The calculation process of which is shown in equation (1) [16].

$$\varphi_{a,b}(t) = |a|^{-\frac{1}{2}} \varphi(\frac{t-a}{b}), a, b \in R, a \neq 0 \tag{1}$$

In equation (1), φ denotes the fundamental wavelet, a denotes the expansion factor, b denotes the translation factor, and $\varphi_{a,b}$ denotes the continuous wavelet. The variation form of continuous wavelet is shown in equation (2).

$$W_{f(a,b)} = \langle f, \varphi_{a,b} \rangle = |a|^{-\frac{1}{2}} \int_R f(t)\phi(\frac{t-b}{a})dt \tag{2}$$

In equation (2), $\langle f, \varphi_{a,b} \rangle$ denotes the inner product of the two and $\phi(t)$ denotes the conjugate complex. The time domain analysis of a signal allows mapping of a one-dimensional time signal into a two-dimensional plane on the time axis and frequency group layers. The formula for this process is shown in equation (3).

$$f_a = f_c \times \frac{f_s}{a} \tag{3}$$

In equation (3), f_s denotes the centre frequency of the wavelet, f_c denotes the sampling frequency and f_a denotes the actual frequency. Different wavelet functions show different effects on time-frequency thermograms, therefore, in order to select the most effective thermograms, the study adopts Tamura texture for feature extraction. Because Tamura texture can effectively capture the subtle texture features of an image with high differentiation and stability, it is suitable for time-frequency heat map analysis of signals. Compared to other texture features, Tamura texture provides more accurate and reliable characterization in time-frequency thermogram presentation. Tamura texture mainly considers six dimensions of the image, which are orientation, roughness, linearity, contrast, roughness, and regularity. Among them, the formula for orientation degree is shown in equation (4).

$$F_{dir} = \begin{cases} |\Delta G| = (|\Delta_H|) + (|\Delta_V|) \\ \theta = \tan^{-1}(|\Delta_V| / |\Delta_H|) + \frac{\pi}{2} \end{cases} \tag{4}$$

In equation (4), Δ_V and Δ_H denote the amount of gradient change of the texture image in the vertical and horizontal directions, respectively. The formula for roughness is shown in equation (5).

$$F_{crs} = \frac{1}{m \times n} \sum_{i=1}^{m} \sum_{j=1}^{n} S_{best}(i,j) \tag{5}$$

In equation (5), $S_{best}(i,j)$ denotes the optimal image grain size at the two-dimensional coordinate point (i,j), m denotes the image length, and n denotes the image width. The formula for calculating the degree of linearity is shown in equation (6).

$$F_{lin} = \frac{\sum_{i}^{n} \sum_{j}^{n} P_{Dd}(i,j) \cos\left[(i,j)\frac{2\pi}{n}\right]}{\sum_{i}^{n} \sum_{j}^{n} P_{Dd}(i,j)} \tag{6}$$

In equation (6), $P_{Dd}(i, j)$ denotes the symbiotic matrix distance points in 2D coordinates (i, j). The contrast calculation formula is shown in equation (7).

$$Fcon = \frac{\sigma}{(\mu_4/\sigma^4)^{\frac{1}{4}}} \tag{7}$$

In equation (7), σ denotes the image grey scale standard, and σ^2 denotes the variance. μ_4 denotes the fourth order mean. The formula of regularity is shown in equation (8).

$$F_{reg} = 1 - r(\sigma_{crs} + \sigma_{con} + \sigma_{dir} + \sigma_{lin}) \tag{8}$$

In equation (8), σ_{crs}, σ_{con}, σ_{dir} and σ_{lin} denote the standard deviation of roughness, contrast, directionality and linearity, respectively, and the roughness calculation formula is shown in equation (9).

$$F_{rgh} = F_{crs} + F_{con} \tag{9}$$

The meaning of each expression in equation (9) is the same as explained previously. Since the time-frequency thermograms have the same background colour, it leads to some challenges in classifying the pixels with deviations in them. The commonly used image enhancement methods are spatial and frequency domains, therefore, the study chooses the binarisation technique in the frequency domain as the enhancement means. Because binarization can effectively convert the time-frequency thermogram into a black-and-white image, highlighting the differences between different frequency components, making the fault characteristics clearer and more explicit, and suitable for rapid and intuitive identification of fault modes. Compared with other techniques, binarization is simple and easy to implement, and it can retain the main frequency information, which improves the recognition accuracy and visualization effect of the image. And the derivation of the binarisation process is shown in equation (10) [17].

$$\begin{cases} a_0 = N_0/(m \times n) \\ a_1 = N_1/(m \times n) \end{cases} \tag{10}$$

In equation (10), a_0 and a_1 denote the percentage of foreground and background pixel distributions in the global, N_0 and N_1 denote the number of pixel grey levels less than and greater than the threshold pixel point. The final binarisation formula is obtained as shown in equation (11).

$$g = a_0 a_1 (\beta_0 - \beta)^2 + a_1 (\beta_1 - \beta)^2 \tag{11}$$

In equation (11), β_0 and β_1 denote the average grey level of pixels in the foreground and background, respectively, and g denotes the inter-class variance. The video feature enhancement map after binarisation is shown in Figure 2.

Figure 2(a) shows the initial time-frequency feature map. Figure 2(b) shows the first valued feature map. Figure 2(c) shows the second valued feature map, and Figure 2(d) shows the critical time-frequency feature map. As can be seen from Figure 2, the initial more dispersed time-frequency feature image, after two binarisation processes, in which the key feature factors are centrally extracted and characterised. It shows

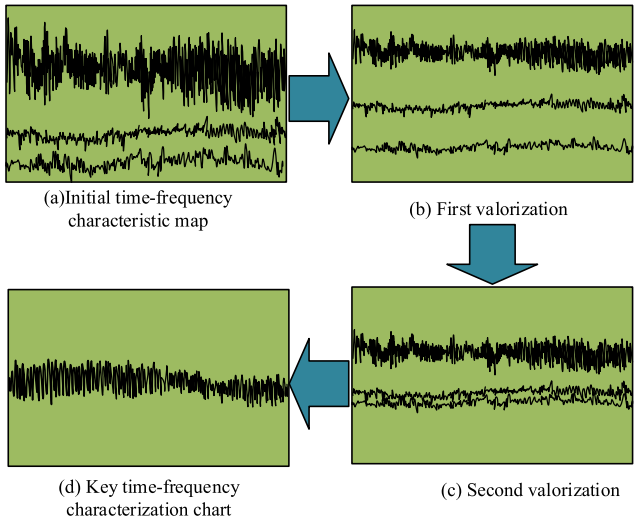

FIGURE 2. Time frequency feature image after feature enhancement.

that this technique can separate various frequencies and their distribution laws from the image background and achieve the segmentation of the target and the background, so as to strengthen the distribution of the frequency components and improve the recognition rate and operation speed in the later stage.

B. FAULT MONITORING AND DIAGNOSIS MODEL CONSTRUCTION BY COMBINING LBP AND SVM

After obtaining the enhanced thermal map of the motor signal, the study adopts the idea of LBP for feature extraction analysis of the time-frequency distribution map before and after the occurrence of faults. LBP compares each pixel in the image with its neighbouring pixels, and generates a local binary pattern based on the result of the comparison. This local binary pattern describes the luminance relationship between a pixel point and its surrounding pixels, which is encoded as a binary number, and this encoded binary number can be used to represent the texture features. The schematic diagram of the LBP operation process is shown in Figure 3.

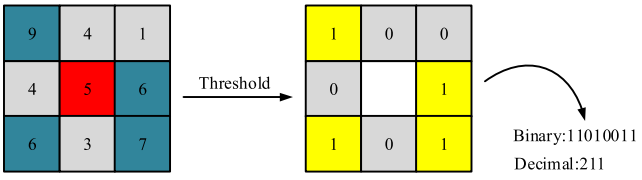

FIGURE 3. LBP operation diagram.

As can be seen in Figure 3, the central number 5 is used as the threshold point and the surrounding numbers are compared to it. If it is greater than the threshold, it is labelled as 1 and if it is less than the threshold, it is labelled as 0. Thus an eight digit binary number is obtained and there are a total of 256 possibilities for combining these numbers. For simplicity of operation, the representation is changed to

a decimal number, i.e., the LBP code. The computational formula for the LBP code is shown in equation (12).

$$LBP(x, y) = \sum \{n = 0\} \wedge \{P - 1\} s(n) \ * 2 \wedge n \quad (12)$$

In equation (12), (x, y) denotes the coordinates of the center pixel; P denotes the number of pixel points contained in the neighborhood centered on the center pixel, which is usually the number of points on a circular neighborhood. The radius R denotes the radius of the neighborhood, i.e., the radius of the neighborhood circle centered on the center pixel. Typically, the relationship between P and R is $P = 8^*R$. $s(n)$ denotes the binarization result obtained by comparing with the grayscale value of the center pixel, if the grayscale value of the neighboring point is greater than or equal to the grayscale value of the center pixel, $s(n)$ takes the value of 1, and 0 otherwise. SVM is mainly used in classification problems, and its core idea is to find a maximal spacing hyperplane, i.e., a decision boundary that maximises the spacing between data points of different classes [18]. A linearly divisible SVM can divide two classes of data by a plane that maximises the interval between the divisions [19]. The schematic diagram of linearly divisible SVM is shown in Figure 4.

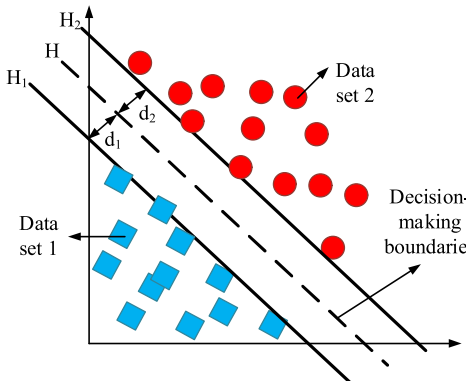

FIGURE 4. Schematic diagram of linearly separable SVM.

As can be seen from Figure 4, a simple dataset is divided into two types of datasets with red circles and blue squares by a dotted line. And this dotted line is the decision boundary of SVM. The data points that are closer to the decision boundary are called support vectors, and in order to define this decision boundary [20]. Generally, two parallel lines with intervals of d_1 and d_2 are chosen to approximate the truest decision boundary by infinitely deriving these two lines. The formula for this process is shown in equation (13).

$$D = \{(x_i, y_i) | i = 1, 2, \cdots, n\}, x_i \in R, y_i \in \{1, -1\} \quad (13)$$

In equation (13), D denotes a complete data set, x_i and y_i denote two 2D data points on the data set, respectively. The formula for this data set to be correctly linearly classified is shown in equation (14).

$$wx + b = 0 \quad (14)$$

In equation (14), w and b both belong to the weights and biases of the samples in the given data set, and x represents the feature space. Then the distance between two parallel lines and the decision boundary is calculated as shown in equation (15).

$$\begin{cases} d1 = \frac{|wx+b|}{\|w\|} = \frac{1}{\|w\|} \\ d2 = \frac{2}{\|w\|} \end{cases} \quad (15)$$

The variables of interest in equation (15) are consistent with the interpretation between. However, problems that cannot be classified by a two-dimensional straight line need to be mapped to a high-latitude environment before classification. The method generally transforms the data from low to high latitude in the form of vector points, and the schematic of the linearly indivisible SVM is shown in Figure 5.

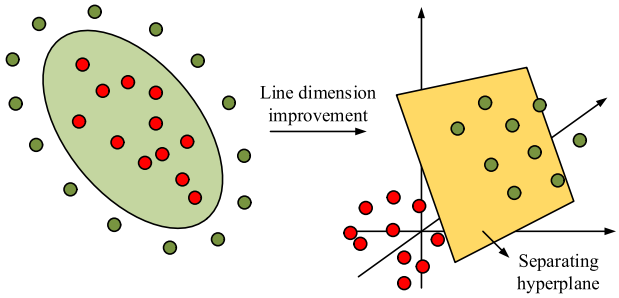

FIGURE 5. Schematic diagram of linearly indivisible SVM.

As can be seen from Figure 5, SVM can map the 2D spatial dataset in the left part to 3D space, and at the same time, due to the greater divisibility of the data in the high-latitude environment, the effective division of the original data can be completed. In the process, the auxiliary processing of kernel function is generally required. The efficiency of mapping and classification can be improved and the complexity of operation can be reduced by choosing appropriate kernel functions. Therefore, the focus of the computational process should be on the kernel function rather than the mapping itself. Common kernel functions include linear Linear kernel function, polynomial Poly, Gaussian radial basis RBF kernel function and Sigmoid kernel function. Considering that the object of this study is motor faults, after combining the number of samples and the number of features, the study combines LBP and SVM with RBF kernel function. Because the RBF kernel function has strong nonlinear mapping ability, it is more effective in dealing with complex nonlinear problems, and is suitable for data with complex time-frequency characteristics such as motor signals. Compared to other kernel functions, the RBF kernel function is able to better capture the nonlinear relationship between the data. And proposes a new motor fault monitoring and diagnostic model using time-frequency thermograms of the motor signals for human-computer analysis. The schematic of the operation flow of the model is shown in Figure 6.

As can be seen from Figure 6, the operation process of the LBP-SVM model can be roughly divided into four parts.

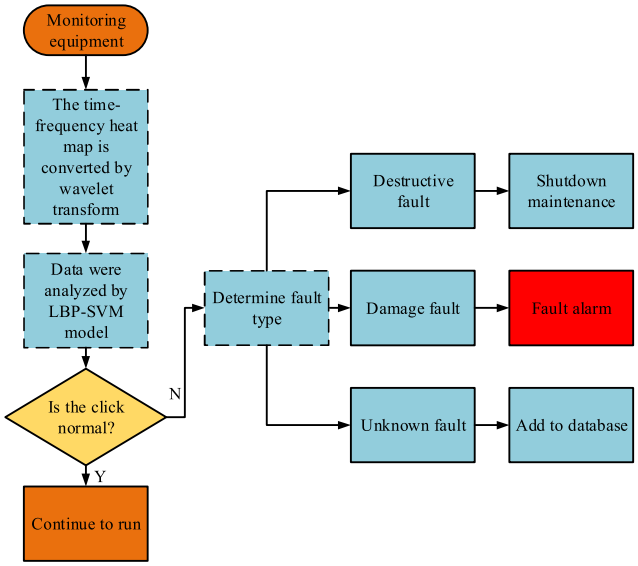

FIGURE 6. The motor operation fault monitoring and diagnosis model combined with LBP-SVM.

Firstly, the motor equipment is monitored for its operation status and data information is collected in real time. Then these collected data are converted into time-frequency thermograms by wavelet transform. Then the data is classified and analysed by LBP-SVM model to filter out the error characteristic data with motor faults, and if there is no such data, the motor continues to work normally. If there is fault data, the type of fault is judged to be destructive, simple damage or unknown. If the fault is destructive, it is necessary to immediately suspend motor operation and start manual maintenance. If it is a minor damaging fault, a fault warning is issued. If it is an unknown type of fault, the fault information is sent to the information base to facilitate subsequent data tracking.

IV. EXPERIMENTAL ANALYSIS OF FAULT MONITORING AND DIAGNOSTIC MODELS

In order to test the performance effect of LBP-SVM model, the first section of the study firstly tested the training of LBP feature extraction and compared the performance of the same type of model, and secondly tested the in-depth classification performance of SVM model. The second section of the study builds a simulation environment and performs simulation tests on the LBP-SVM model.

A. FAULT MONITORING AND DIAGNOSTIC MODEL PERFORMANCE TEST

Motor fault monitoring and diagnostics are critical to ensuring the reliability and efficiency of modern industrial systems. Early identification and accurate diagnosis of faults can significantly reduce unplanned downtime, lower maintenance costs and increase productivity. In order to verify the performance effect of the LBP-SVM diagnostic model, the study builds a suitable experimental environment. The motor fault simulation platform developed by Zongyuan Measurement Company was used for fault diagnosis testing. The vibration signal is collected by 6 acceleration sensors, the data sampling frequency is set to 53000 Hz, the rated speed of the motor is set to 1520 r/min, and the power supply frequency is set to 80 Hz. The motor test stand is shown in Figure 7.

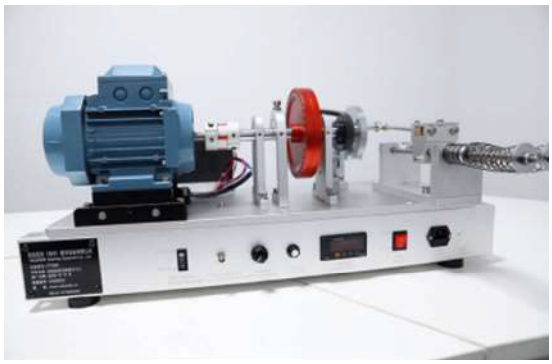

Motor Failure Test Bench

FIGURE 7. Image of motor test bench.

As can be seen in Figure 7, the test stand includes a standard industrial motor connected to the load to simulate operating conditions and is equipped with a variable frequency drive to control the motor speed, allowing for both fixed and variable speed testing. Data acquisition was performed using an array of high-precision sensors, including vibration, temperature, and current sensors, which were mounted at strategic locations on the motor and load assembly. The collected data is then digitized by a high-speed data logger, ensuring that the motor's operating characteristics are accurately captured under a wide range of fault conditions, including bearing failures, misalignment and unbalanced loads. The number of samples for each type of fault data is 12, and the length of the samples is 1 s. A total of 500 pieces of data after sampling for 40 min are divided into the training set and the test set according to the ratio of 8:2, and the recognition accuracy is taken as the reference index. Taking the recognition accuracy as the reference index, the LBP, Local Directional Pattern (LDP), Local Phase Quantization (LPQ), and HOG feature extraction. LBP, Local Directional Pattern (LDP), Local Phase Quantisation (LPQ) and HOG feature extraction method (Histogram of Oriented Gradient). The specific test results are shown in Figure 8.

Figure 8(a) shows the feature recognition accuracy results of the four models on the training set, and Figure 8(b) shows the feature recognition accuracy results of the four models on the test set. As can be seen from Figure 8, there is a decreasing trend in the combined recognition ability of all four models on the training set, but overall, the LBP model has the slowest decreasing trend. In the test set, the feature recognition accuracy of the LBP model is the highest, with a maximum value of about 90%. This result points to the effectiveness of LBP feature extraction in handling motor fault data. Compared to other feature extraction methods, the LBP method is more

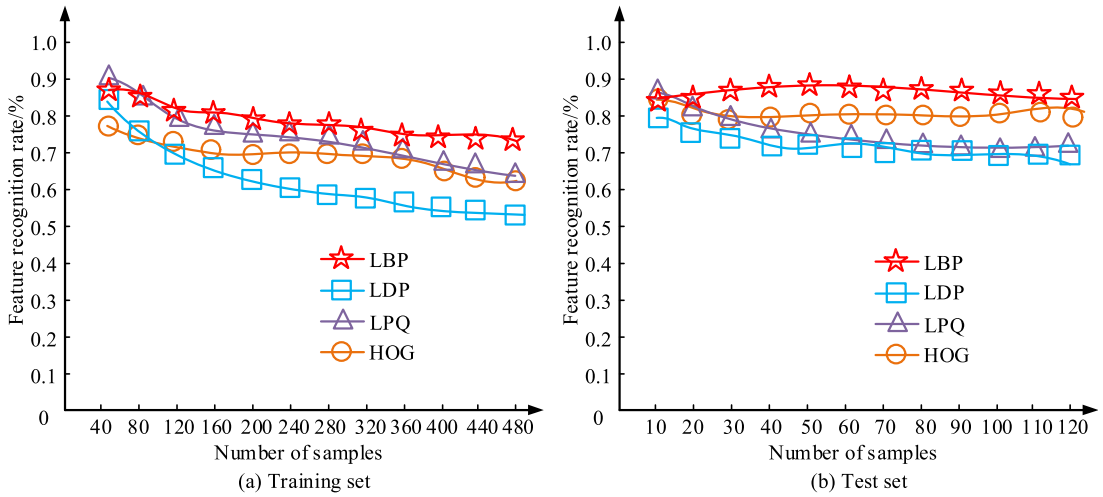

FIGURE 8. Training test results of different feature extraction models.

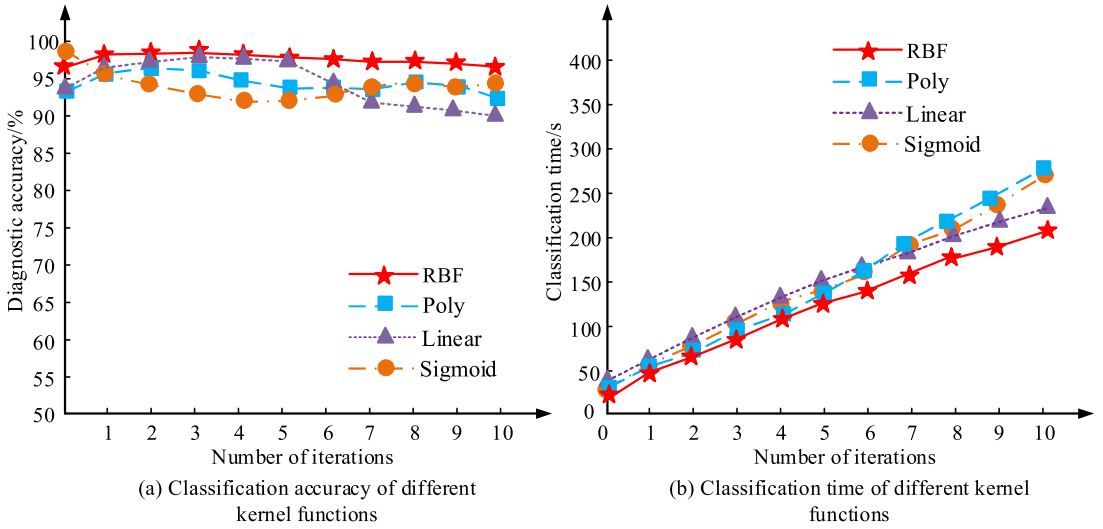

FIGURE 9. Testing the diagnostic accuracy and classification speed of different kernel functions.

sensitive and accurate in capturing motor fault features. After comparatively testing the signal recognition performance of the different models, the study continued with comparative testing of the signal feature classification models. Taking the diagnosis correctness and classification time as the reference index, the test results for different kernel functions, such as Poly kernel function, RBF kernel function, Linear kernel function and Sigmoid kernel function, are shown in Figure 9.

Figure 9(a) shows the fault diagnosis accuracy under four different kernel functions, and Figure 9(b) shows the classification speed under four different kernel functions. As can be seen from Figure 9, the diagnosis accuracy of the four kernel functions does not differ much with the increase in the number of iterations, and the best performance is the RBF kernel function, which has the highest fault diagnosis rate of about 97%. In addition, as the number of iterations increases, the time required for different kernel functions to complete the classification task increases gradually. Among them, the RBF kernel function has the least time of 200 seconds, which is about 80 seconds earlier than the Poly kernel function. The reason for this may be that the RBF kernel function can map the samples to a high dimensional space, but it requires fewer parameters compared to the Poly kernel function, so the training time is shortened and more time-saving. In summary, the study is based on the RBF kernel function, 80 data are randomly selected from the fault data samples as fault samples, and the other 80 data are also randomly selected from the data samples of the normal operation of the motor as normal data samples. The time-frequency diagram before dichotomous reinforcement, the time-frequency diagram after dichotomous reinforcement, Laplace sharpening and morphological processing are compared with the

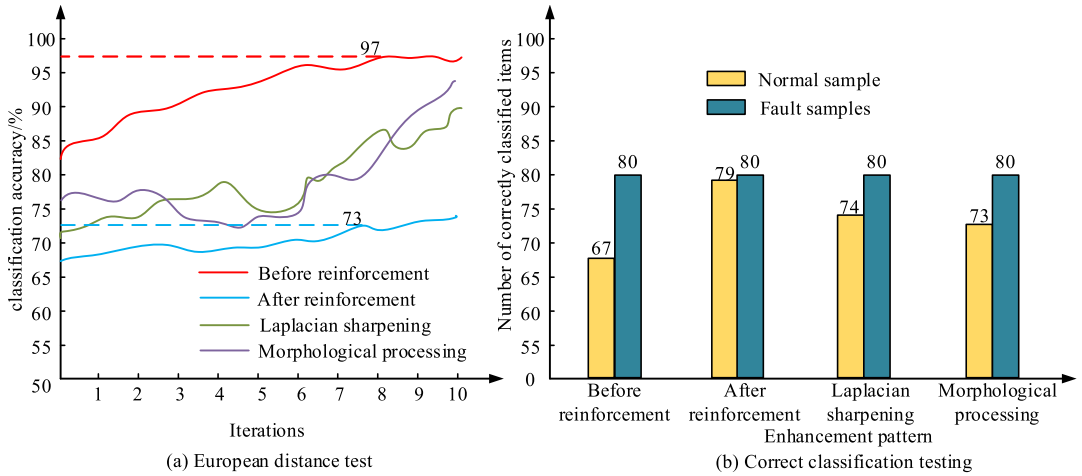

FIGURE 10. Test results of different signal reinforcement methods.

TABLE 1. Motor operating parameters table.

Collection location	Speed (r/min)	Fault type	Fault diameter/mm	Sampling frequency/Hz
Driving end	1530, 1550, 1572	No	No	48 K
Driving end	1530	Outer ring pitting	0.177	48 K
Driving end	1550	Outer ring pitting	0.356	48 K
Driving end	1572	Outer ring pitting	0.524	48 K
Driving end	1530	Inner ring pitting	0.179	48 K
Driving end	1550	Inner ring pitting	0.367	48 K
Driving end	1572	Inner ring pitting	0.571	48 K
Driving end	1530	Rolling body pitting	0.167	48 K
Driving end	1550	Rolling body pitting	0.352	48 K
Driving end	1572	Rolling body pitting	0.602	48 K

classification accuracy as the reference index. The test results are shown in Figure 10.

Figure 10(a) shows the classification accuracy test results under different image enhancement methods, and Figure 10(b) shows the actual fault classification test results under different image enhancement methods. As can be seen from Figure 10, the fault classification accuracy after binary reinforcement is significantly improved up to 97%. Compared with the time-frequency feature map before reinforcement, the efficiency is improved by 34%. Meanwhile the classification accuracy of other reinforcement methods is significantly lower than that of the time-frequency feature map after reinforcement. In addition, for different feature reinforcement methods, after diagnosing 80 motor normal operation sample data, it is found that the diagnosis data after binary reinforcement is 79, and the diagnosis efficiency is better than other methods. The reason for this is that binarization reinforcement helps to highlight important features in the image, making it easier for the classifier to distinguish between different fault types. In contrast, other reinforcement methods may not highlight fault-related features.

B. FAULT MONITORING AND DIAGNOSTIC MODEL SIMULATION TEST

The study used Case Western Reserve University's motor bearing operation database to simulate and test the LBP-SVM model proposed in this study, which used a motor test bed with a motor power of 1521 W and two sampling frequency settings of 12 kHz and 48 kHz. A pair of torque sensors was used at the motor output position to collect the output data and monitor the motor operation status in real time under the miner's operation. The faults are implanted by EDM single-point damage, and the implanted faults are of different complexity and in different locations of the motor bearings. The general motor bearing faults are divided into three kinds: inner ring faults, outer ring faults, rolling body faults. The specific experimental motor parameters are shown in Table 1.

Table 1 shows that under the same data acquisition position, acquisition frequency and the same motor bearing speed, different fault types result in different fault diameters. However, as the bearing speed increases, the fault diameter becomes larger and larger. In addition, under the same collection position, sampling frequency and rotational speed,

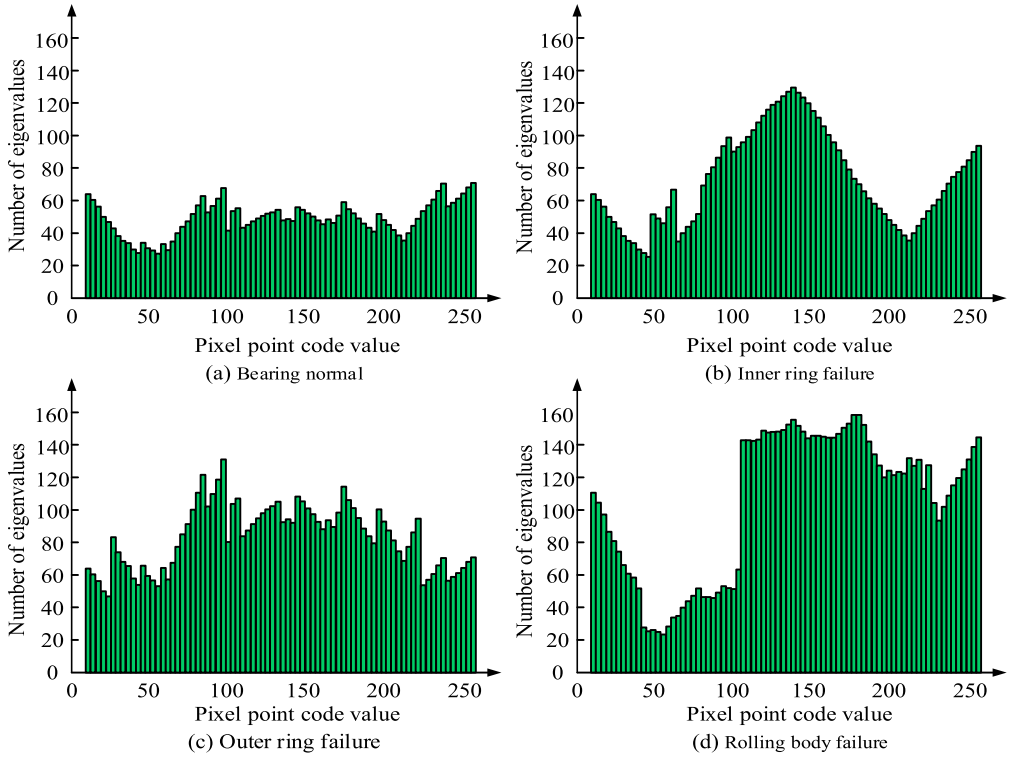

FIGURE 11. Histogram of characteristics for different fault types.

the fault diameter of rolling element pitting is significantly larger than that of inner ring pitting, and outer ring pitting. The above results illustrate that for variable-speed operation modes, the LBP-SVM model proposed by the study is particularly applicable and can adapt to these feature changes, ensuring that the model can still accurately diagnose motor faults under variable-speed conditions. In order to demonstrate the feasibility of the proposed method under different environments in a more graphic way, the study plots the local binary feature cases of the time-frequency thermograms of the motor bearings with normal, inner-ring faults, outer-ring faults, and rolling-body faults in the form of feature histograms with feature-enhanced processing. The test results are shown in Figure 11.

Figure 11(a) is the histogram of the characteristics of the bearing normal. Figure 11(b) is the histogram of the characteristics of the failure of the inner ring. Figure 11(c) is the histogram of the characteristics of the failure of the outer ring. Figure 11(d) is the histogram of the characteristics of the rolling element failure. As can be seen from Figure 11, the normal eigenvalue of the bearing is generally in a smooth state, and the maximum eigenvalue is not more than 80, and there are obvious random fluctuations in the eigenvalue change after the failure. The maximum eigenvalue of inner ring failure is close to 130, the maximum eigenvalue of outer ring failure is close to 130, and the maximum eigenvalue of rolling element failure is close to 160. The performance of this data is similar to Table 2. It can be seen that the proposed LBP-SVM performs well in many types of faults and has a certain degree of reliability. In order to further verify the authenticity of the above data, the fault data of the inner ring and rolling element of the bearing were re-collected under the same working conditions. The sliding window method is used to split these data, that is, every 1 second split to get 8 data, and the percentage of the calculated results will be output. The test results are shown in Figure 12.

Figure 12(a) shows the fault detection results of the LBP-SVM model for rolling body, and Figure 12(b) shows the fault detection results of the LBP-SVM model for bearing inner ring. As can be seen from Figure 12, under the interference of multiple fault types, the accuracy rate of successfully identifying the fault types of the rolling body is close to 95%, while the accuracy rate of successfully identifying the fault types of the inner ring of the bearing is close to 90% by the fault detection analysis of LBP-SVM. This data is consistent with the conclusion in Table 1 that under the same conditions the fault type identification of rolling body is greater than that of bearing inner ring, followed by outer ring. It shows that the LBP-SVM model proposed by the study is effective for fault diagnosis of motor bearings. Finally, the study to combine these data analysis results with Mean Squared Error (MSE).

Root Mean Squared Error (RMSE) and Mean Absolute Error (MAE) are used as reference indexes to compare and test existing fault diagnosis models, which include POS-SVM model combined with particle swarm algorithm, Transfer Learning (TL) model, Current Monitoring (CM) model,

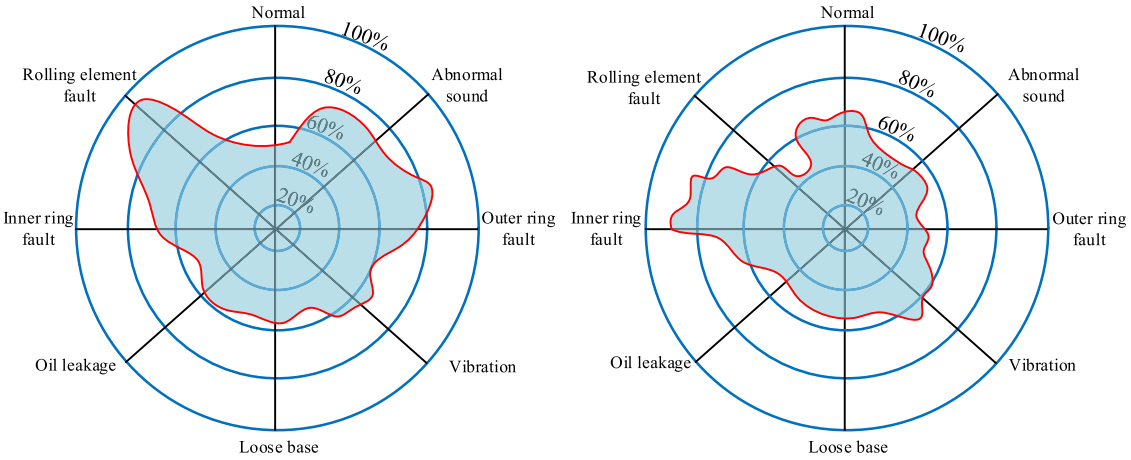

(a) Rolling element fault analysis

(b) Fault analysis of bearing inner ring

FIGURE 12. LBP-SVM model fault detection results.

TABLE 2. Test results of different fault diagnosis models.

Method	MSE	RMSE	MAE
POS-SVM	0.036	0.444	0.036
Transfer Learning	0.067	0.892	0.058
Current monitoring	0.055	1.213	0.094
Time Domain	0.057	0.548	0.075
LTP-SVM	0.021	0.257	0.026
GRU-SVM	0.025	0.289	0.088
D-q axis current diagnosis [5]	0.054	0.521	0.057
Gabor+Convolutional Network [6]	0.043	0.443	0.063
Dynamic routing diagnosis [7]	0.034	0.387	0.031
Local ternary+grayscale co-occurrence [8]	0.024	0.297	0.035
Circular local binary diagnosis [11]	0.028	0.312	0.041
LBP-SVM	0.017	0.214	0.011

and TL model, Time Domain (TD) model, LTP-SVM model combining local ternary patterns and GRU-SVM combining gated neural units and related literature methods in the review section, etc. The specific test results are shown in Table 2.

As can be seen from Table 2, LTP-SVM, GRU-SVM and POS-SVM have superior metrics test results relative to other non-SVM combined algorithm models. It can be shown that the powerful fault prediction and classification ability of combined SVM makes the comprehensive performance of the model significantly improved. The quantified data shows that the proposed LBP-SVM model has the best overall performance, and among the five diagnostic models, it has the smallest values of MSE, RMSE and MAE, with the smallest MSE of 0.017, the smallest RMSE of 0.214, and the smallest MAE of 0.011. Compared with the current monitoring model, which has the largest value, the value of the model has decreased significantly. In summary, the LBP-SVM model performs well in both image feature extraction and fault classification, and lays a new theoretical foundation for the field of motor operation fault diagnosis. The reasons can be summarized as the following three points, firstly, the LBP algorithm is able to effectively capture the local texture features of an image or a signal, which are crucial for identifying abnormal conditions in motor operation. Second, SVM, especially the RBF kernel function, makes it possible for different classes of data to be effectively classified by mapping the data into a higher dimensional space. Third, the diagnostic accuracy of the model is further improved by means of binary reinforcement, Laplace sharpening and morphological processing of the signal.

V. CONCLUSION

Electric motors play a key role in modern industrial production, and the monitoring of their reliability and operating status is crucial to productivity and equipment safety. With the increasing size of motor systems and the complexity of operating environments, the monitoring and diagnosis of motor faults have become more and more urgent. Firstly, the high dimensional feature space is constructed by collecting the frequency information of the motor during operation and extracting the texture features using LBP technique. Then, the motor state is classified and diagnosed with the help of SVM supported by Gaussian kernel function. The experimental results show that the highest value of feature recognition accuracy of LBP model is about 90%. The shortest time for the SVM model combined with the RBF kernel function to complete the feature classification is 200. The accuracy of the fault classification of the time-frequency feature map after the binary enhancement is up to 97%, which is 34% more efficient compared to the efficiency before the enhancement. Simulation tests found that the accuracy of the LBP-SVM

model in successfully identifying rolling body fault types is close to 95%, and the accuracy of successfully identifying bearing inner ring fault types is close to 90%. Its MSE is at least 0.017, RMSE is at least 0.214, and MAE is at least 0.011. In summary, the proposed model of the study reaches the industry-leading level in all the indexes, which demonstrates the model's remarkable results in the monitoring and diagnosis of electric motor faults. A highlight of the research is the improvement of LBP and the combination of SVM, which reduces the dependence on large-scale training data, provides strong technical support for motor fault prevention and maintenance, and is of great significance in promoting the development of motor fault diagnosis technology. In the future, the research will continue to deepen the application of LBP and SVM in electric motor fault diagnosis, and explore the combination of more feature extraction and classification methods to adapt to more complex working environments and fault patterns. The integration of deep learning techniques will also be considered to further enhance the performance and universality of fault diagnosis.

REFERENCES

[1] R. Ma, T. Han, and W. Lei, "Cross-domain meta learning fault diagnosis based on multi-scale dilated convolution and adaptive relation module," *Knowledge-Based Syst.*, vol. 261, Feb. 2023, Art. no. 110175.
[2] Y. Ma, J. Yang, and L. Li, "Collaborative and adversarial deep transfer auto-encoder for intelligent fault diagnosis," *Neurocomputing*, vol. 486, pp. 1–15, May 2022.
[3] M. Rajalakshmi and K. Annapurani Panaiyappan, "A multimodal architecture using adapt-HKFCT segmentation and feature-based chaos integrated deep neural networks (Chaos-DNN-SPOA) for contactless biometricpalm vein recognition system," *Int. J. Intell. Syst.*, vol. 37, no. 3, pp. 1846–1879, Mar. 2022.
[4] Y. Li, Y. Luo, X. Gu, D. Chen, F. Gao, and F. Shuang, "Point cloud classification algorithm based on the fusion of the local binary pattern features and structural features of voxels," *Remote Sens.*, vol. 13, no. 16, p. 3156, Aug. 2021.
[5] X. Jiang, S. Wang, J. Li, D. Wu, W. Huang, and Z. Han, "A strong robustness open-circuit fault diagnosis strategy for novel fault-tolerant electric drive system based on d-q-axis current signal," *Chin. J. Aeronaut.*, vol. 34, no. 10, pp. 115–127, Oct. 2021.
[6] S. Afrasiabi, M. Mohammadi, M. Afrasiabi, and B. Parang, "Modulated Gabor filter based deep convolutional network for electrical motor bearing fault classification and diagnosis," *IET Sci., Meas. Technol.*, vol. 15, no. 2, pp. 154–162, Mar. 2021.
[7] P. Fu, J. Wang, X. Zhang, L. Zhang, and R. X. Gao, "Dynamic routing-based multimodal neural network for multi-sensory fault diagnosis of induction motor," *J. Manuf. Syst.*, vol. 55, pp. 264–272, Apr. 2020.
[8] F. Behloul, F. Tafinine, and O. Yaman, "Induction motor fault diagnosis with local ternary pattern and AI approaches," *J. Failure Anal. Prevention*, vol. 23, no. 6, pp. 2533–2541, Dec. 2023.
[9] V. Hernandez-Ramirez, D.-L. Almanza-Ojeda, J.-J. Cardenas-Cornejo, J.-L. Contreras-Hernandez, and M.-A. Ibarra-Manzano, "Detection of broken bars in induction motors using histogram analysis of current signals," *Appl. Sci.*, vol. 13, no. 14, p. 8344, Jul. 2023.
[10] M. Basaran and M. Fidan, "Induction motor fault classification via entropy and column correlation features of 2D represented vibration data," *Eksploatacja I Niezawodnosc Maintenance Rel.*, vol. 23, no. 1, pp. 132–142, Mar. 2021.
[11] I. Al Saidi, M. Rziza, and J. Debayle, "A novel texture descriptor: Circular parts local binary pattern," *Image Anal. Stereology*, vol. 40, no. 2, pp. 105–114, Jul. 2021.
[12] J. Zhu, S. Li, Q. Ma, B. He, and J. Song, "Support vector machine-based rapid magnitude estimation using transfer learning for the Sichuan–Yunnan region, China," *Bull. Seismological Soc. Amer.*, vol. 112, no. 2, pp. 894–904, Apr. 2022.
[13] W. Qin, G. Fan, and Hongxing-Li, "Estimation and predicting of soil water characteristic curve using the support vector machine method," *Earth Sci. Informat.*, vol. 16, no. 1, pp. 1061–1072, Mar. 2023.
[14] B. Cui, Y. Weng, and N. Zhang, "A feature extraction and machine learning framework for bearing fault diagnosis," *Renew. Energy*, vol. 191, pp. 987–997, May 2022.
[15] N. Jiao, X. Han, Z. Wei, C. Sun, P. Liang, and W. Liu, "Online fault diagnosis for rotating rectifier in wound-rotor synchronous starter–generator based on geometric features of current trajectory," *IEEE Trans. Ind. Electron.*, vol. 68, no. 4, pp. 2952–2963, Apr. 2021.
[16] F. Masood, J. Masood, H. Zahir, K. Driss, N. Mehmood, and H. Farooq, "Novel approach to evaluate classification algorithms and feature selection filter algorithms using medical data," *J. Comput. Cognit. Eng.*, vol. 2, no. 1, pp. 57–67, May 2022.
[17] M.-C. Kim, J.-H. Lee, D.-H. Wang, and I.-S. Lee, "Induction motor fault diagnosis using support vector machine, neural networks, and boosting methods," *Sensors*, vol. 23, no. 5, p. 2585, Feb. 2023.
[18] J.-G. Jang, C.-M. Noh, S.-S. Kim, S.-C. Shin, S.-S. Lee, and J.-C. Lee, "Vibration data feature extraction and deep learning-based preprocessing method for highly accurate motor fault diagnosis," *J. Comput. Design Eng.*, vol. 10, no. 1, pp. 204–220, Jan. 2023.
[19] U. Scherhag, J. Kunze, C. Rathgeb, and C. Busch, "Face morph detection for unknown morphing algorithms and image sources: A multi-scale block local binary pattern fusion approach," *IET Biometrics*, vol. 9, no. 6, pp. 278–289, Nov. 2020.
[20] H. Tang, S. Lu, G. Qian, J. Ding, Y. Liu, and Q. Wang, "IoT-based signal enhancement and compression method for efficient motor bearing fault diagnosis," *IEEE Sensors J.*, vol. 21, no. 2, pp. 1820–1828, Jan. 2021.

WENCHANG WU received the M.S. degree in circuits and systems from the School of Electronic Engineering, University of Electronic Science and Technology of China, in 2011. Since 2012, he has been with the School of Automotive and Electromechanical Engineering, Xinyang Vocational and Technical College. His current primary research interests include electric vehicle electronic control technology, deep learning, and intelligent fault diagnosis.